Theoretical study of ion-pair formation and Penning and associative ionization in low- to intermediate-energy $He^*(2^{1,3}S)+Li$ collisions

M. Kimura
Argonne National Laboratory, Argonne, Illinois 60439
and Department of Physics, Rice University, Houston, Texas 77251

N. F. Lane
Department of Physics, Rice Quantum Institute, Rice University, Houston, Texas 77251
(Received 9 January 1990)

A semiclassical treatment based on a molecular orbital expansion is used to study ion-pair formation and Penning- and associative-ionization processes in $He^*(2^{1,3}S)+Li$ collisions in the energy regime from 100 to 1000 eV. Although these processes are usually important in different energy ranges, here they are found to compete with each other to an appreciable degree and hence to provide a rare opportunity for investigating collision dynamics that require an equal-footing treatment between autoionization to the continuum and a discrete transition. The present cross sections for these processes compare favorably with the measurement of Wang, Tang, and Neynaber [J. Phys. B **20**, 1527 (1987)].

I. INTRODUCTION

Ion-pair formation (IPF) in collisions involving alkali-metal atoms has been a subject of extensive experimental and theoretical studies in recent years, in part because of its practical application to the production of negative-ion beams.[1-4] In most of these studies, however, a ground-state hydrogen atom is the collision partner for the alkali-metal atom; consequently, the number of probable inelastic channels at low to intermediate energies is quite limited. This limitation is unfortunate from a fundamental point of view. On the other hand, if one of the collision partners is an excited atom whose energy exceeds the ionization threshold of the alkali-metal atom, several new channels, including Penning and associative ionization, are available; the additional channels pose interesting challenges to experimental and theoretical investigation.

Neynaber and his colleagues[5,6] used a merging-beam technique to carry out experiments on simultaneous IPF and Penning- and associative-ionization (PI-AI) processes in collisions of excited He at collision energies up to 1.5 keV. Specifically, they studied the following processes:

$$He^*(2^{1,3}S)+Li \rightarrow He^+ + Li^- \quad (IPF) \tag{1}$$

$$He^*(2^{1,3}S)+Li \rightarrow He+Li^+ + e^- \quad (PI) \tag{2}$$

$$\rightarrow HeLi^+ + e^- \quad (AI)\,. \tag{3}$$

Neynaber and co-workers obtained values for the cross sections of 7.2×10^{-18} cm^2 for IPF [Eq. (1)] and 1.0×10^{-16} cm^2 for total PI-AI [Eqs. (2) and (3)] at a He^* collision energy of 500 eV (laboratory energy).

Since the excitation energy of $He^*(2^{1,3}S)$ far exceeds the ionization energy of Li, the $He+Li^+$ state lies energetically below the initial (He^*+Li) atomic energy levels; hence the system is unstable with respect to PI-AI. On the other hand, the $He^+ + Li^-$ (IPF) levels are about 3–4 eV above the initial levels. Therefore the large qualitative difference between the two measured cross sections, i.e., the dominance of the PI-AI process at low energies, is understandable. We have conducted a systematic study of the IPF [Eq. (1)] and PI-AI [Eqs. (2) and (3)] processes in the energy regime of 100–1000 eV by using a semiclassical treatment of the collision dynamics, based on a molecular-orbital expansion of the electronic wave functions. The PI-AI process is treated by means of complex optical model potentials, where the imaginary parts of the potentials correspond to the adiabatic autoionization rates. The principal objectives of this study are twofold: (i) to describe the collision dynamics of the IPF and PI-AI processes, and (ii) to search for evidence of possible interference between the two.

II. SUMMARY OF THEORY

Since details of the theory have been published elsewhere,[7] only a summary is presented here.

A. Molecular states

The molecular-state electronic wave functions are generated by means of a modified valence-bond configuration-interaction method, with Gaussian-type pseudopotentials[8] used to represent the Li^+ and He^+ cores for the $HeLi^*$ and the Li^+ core for the $HeLi^+$. Hence, only two active electrons are treated explicitly. In the structure calculation, a basis set of Slater-type orbitals (STO's) is used, consisting of 21 STO's for Li and 16 STO's for He. The Slater exponents chosen for triplet He are those of Krauss, Maldonado and Wahl,[9] and those for singlet He were obtained by energy optimization with values of 0.538 and 0.389 for $2s$ and $2p$, respectively. Slater exponents for Li were taken from Stevens, Karo,

and Hiskes.[10] Configurations of 192 and 152 Slater determinants for HeLi* were employed for singlet Σ and Π manifolds, respectively, while those of 157 and 96 Slater determinants for $HeLi^+$ were employed for singlet Σ and Π manifolds, respectively.[11] The accuracy of the present molecular calculation may be gauged by the asymptotic energies, which are within 0.1% of experimental values.

B. Close coupling

1. Coupled equations

The total scattering wave function is expanded in terms of discrete and continuum states, i.e.,

$$\psi(\mathbf{r},t)=\sum_i a_i(t)\phi_i^{\mathrm{MO}}(\mathbf{r},\mathbf{R})F_i(\mathbf{r},\mathbf{R},t) + \sum_{l,m}\int d\epsilon\, a_{\epsilon lm}(t)\phi_{\epsilon lm}^{\mathrm{MO}}(\mathbf{r},\mathbf{R})F_\epsilon(\mathbf{r},\mathbf{R},t) , \quad (4)$$

where $\phi_n^{\mathrm{MO}}(\mathbf{r},\mathbf{R})$ represents discrete or continuum molecular-state electronic wave functions, with MO representing molecular orbital, and $F_i(\mathbf{r},\mathbf{R},t)$ contains all phase factors as well as electron translation factors (ETF's).[7] Here, the contribution due to continuum states, the second term in Eq. (4), is treated by discrete sampling at a variety of discrete energies (discretization), i.e.,

$$\int d\epsilon\, g(\epsilon)\simeq\sum_i w_i g(x_i) , \quad (5)$$

where w_i is an appropriate weighing factor, and by inclusion of molecular-continuum partial waves up to $l=5$.

Following the conventional procedure of substituting Eq. (4) into the time-dependent Schrödinger equation, one can easily obtain a set of first-order, time-dependent, coupled equations,[7]

$$\begin{bmatrix}\dot a_i\\ \dot a_{\epsilon lm}\end{bmatrix}=\sum_{j,\epsilon',l',m'}\begin{bmatrix}v_{i;j} & v_{i;\epsilon'l'm'}\\ v_{\epsilon lm;j} & v_{\epsilon lm;\epsilon'l'm'}\end{bmatrix}\begin{bmatrix}a_j\\ a_{\epsilon'l'm'}\end{bmatrix} , \quad (6)$$

where $v_{i;j}$, $v_{i;\epsilon'l'm'}$, and $v_{\epsilon lm;\epsilon'l'm}$ represent discrete-discrete, discrete-continuum, and continuum-continuum interactions, respectively, and are given in general form as

$$v_{kn}=\left\langle k\left|H_{\mathrm{el}}-i\frac{\partial}{\partial t}\right|n\right\rangle . \quad (7)$$

H_{el} is the electronic Hamiltonian and $\partial/\partial t$ is related to the nuclear momentum.

2. Dynamical couplings

a. Discrete-discrete couplings (the IPF *process).* Nonadiabatic couplings arising from both radial and rotational motions of the nuclei [the second term in Eq. (7)] are responsible for causing inelastic electronic transitions of the system. The ETF's correct the corresponding coupling matrix elements by eliminating asymptotic defects, which are known to cause serious problems. The molecular-orbital (MO) ETF's used here are state dependent and are determined by the optimization procedure.[7]

b. Discrete-continuum couplings (the PI-AI *processes).* Phenomenologically, the possibility of transitions to the ionization continuum can be described by a complex optical potential,

$$V(R)=[U(R)-iW(R)] , \quad (8)$$

and the imaginary part of the potential gives rise to the absorption of the initial atoms, i.e., ionization. In the present case, $W(R)$ represents the autoionization width [the first term in Eq. (7)] and can be approximated simply by[12]

$$W(R)=2\pi\rho_E\sum_{l,m}|\langle\mathcal{A}\phi_j^{AB^+}(\mathbf{r},R)\phi_{\epsilon lm}^{e^-}|H_{\mathrm{el}}|\phi_i^{AB^*}(\mathbf{r},R)\rangle| , \quad (9)$$

where $\phi_i^{AB^*}$ and $\phi_j^{AB^+}\phi_{\epsilon lm}^{e^-}$ are assumed to be orthogonal, ρ_E is the density of states, and $\mathcal{A}$ represents the antisymmetrizer. In the present study, the continuum wave functions were generated by the Hartree-Fock (exact static exchange) approximation to elastic electron scattering from the AB^+ molecular ion.

3. Transition probabilities

As stated earlier, we chose the nonadiabatic coupling with the ETF correction [i.e., second term in Eq. (7)] for discrete-discrete couplings, while the matrix elements [first term in Eq. (7)] that appear in the autoionization width are taken to be the dominant discrete-continuum coupling. We assume that the PI-AI process takes place only from the initial $He(2\,^1S)$ and $He(2\,^3S)$ states. This semiclassical treatment with a straight-line trajectory is considered to be valid at least down to a collision energy of $\sim$100 eV.[7] Molecular states included in the present calculations are the initial $[He(2\,^{1,3}S)+Li]$, $[He(2\,^{1,3}P)+Li]$, $[He(2\,^{1,3}S)+Li(2p)]$, $[He(2\,^{1,3}P)+Li(2p)]$, and $[He(3\,^{1,3}S)+Li(2p)]$ manifolds with respective Σ and Π states for the IPF and 30 different ϵ values between 0.02 and 2.5 a.u. (measured with respect to the energies of the initial channels) for the continuum with l values up to 5 ($m\le 2$) for the PI-AI. All flux transferred into the $[He(2\,^1P)+Li(2p)]$ level is considered to constitute IPF since crossings at large R are assumed to be diabatic.

The probabilities for the IPF and the PI-AI, at a given impact parameter b and energy E are given, respectively, by

$$P_j(E,b)=|a_j(t\to\infty)|^2 \quad \text{(IPF)} \quad (10a)$$

and

$$P_\epsilon(E,b)=\sum_{l,m}\int d\epsilon|a_{\epsilon lm}(t\to\infty)|^2 \quad \text{(PI-AI)} . \quad (10b)$$

III. RESULTS AND DISCUSSION

A. Adiabatic potential-energy curves and coupling matrix elements

Figure 1 displays the adiabatic potential-energy curves for the $[He^*+Li]$ and $HeLi^+$ states, which are labeled

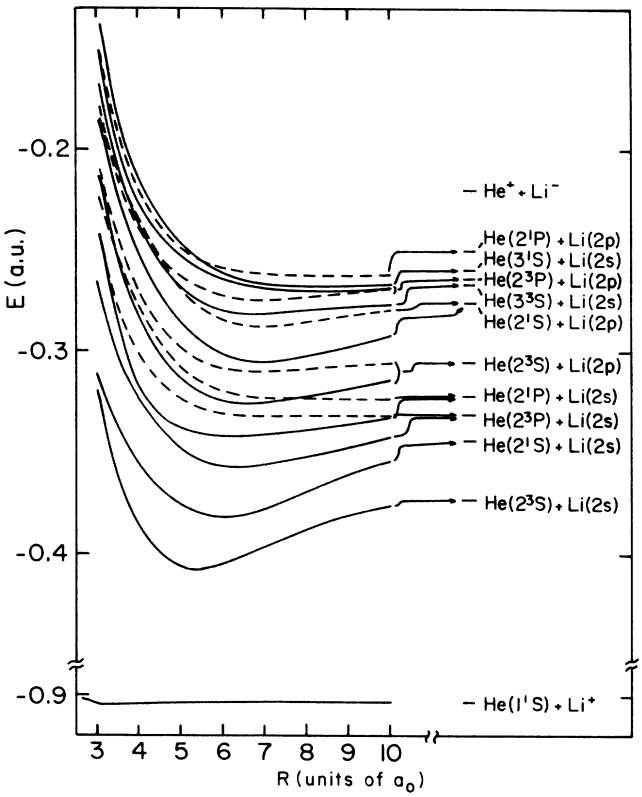

FIG. 1. Adiabatic potentials of the HeLi* and $HeLi^+$ systems. Solid lines are for $^2\Sigma$ and dashed lines for $^2\Pi$. These are labeled $0\Sigma, 1\Sigma, \ldots$ for Σ states and $1\Pi, 2\Pi, \ldots$ for Π states from the lowest level, respectively, for convenience.

$0\Sigma, 1\Sigma, 2\Sigma, \ldots$ and $1\Pi, 2\Pi, \ldots$ starting from the lowest level. Only doublet states, excited from the initial [He($2\,^{1,3}S$)+Li] manifolds, can contribute to the IPF and PI-AI channels; therefore, only $^2\Sigma$ and $^2\Pi$ states are included in Fig. 1. The $^2\Delta$ states are neglected because they play only a minor role in flux redistribution within a given n state.

Because of the weak polarization interaction between the neutral colliding atoms, the potential curves of the low-lying states show no strong avoided crossings, thus suggesting (i) the Demkov-type mechanism for the electron transfer process, and (ii) the ladder-climbing mechanism for a series of excitations leading to IPF. However, the increasingly stronger influence of the [$He^+ + Li^-$] ion-pair configuration on higher-lying states gives rise to avoided crossings at large internuclear distances, thus implying larger probabilities of excitation and electron transfer among these states. In order to reach the IPF level, the flux will predominantly undergo a series of one-electron excitations through the ladder-climbing mechanism, and eventually the excited electron on He will be transferred to Li to form the ion pair. On the other hand, the PI-AI channel is embedded in the continuum at any internuclear distance R; thus PI-AI transition can take place even adiabatically.

Illustrated in Fig. 2 are representative nonadiabatic coupling matrix elements. Radial couplings among low-

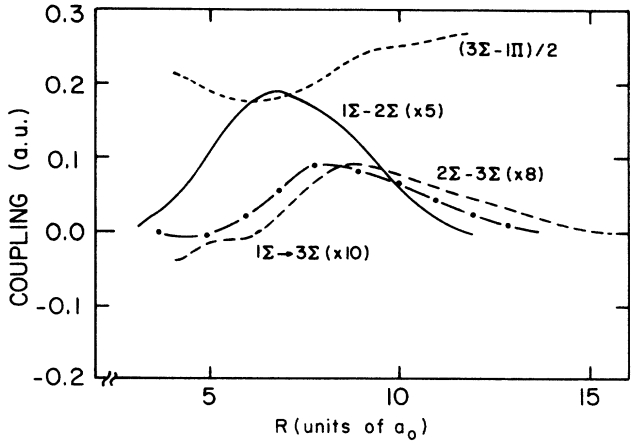

FIG. 2. Representative nonadiabatic radial and rotational couplings.

lying states are very weak, in particular, those connecting the initial channel, although the radial coupling between 1Σ and 2Σ has a peak around $R \simeq 7a_0$. The general shapes of the coupling matrix elements and the positions of the corresponding peaks are typical of those of the Demkov-type coupling scheme.[7] Autoionizing widths from the singlet and triplet manifolds are displayed in Fig. 3. Since we know of no similar published widths for the He*-Li system, we cannot make comparisons. However, extensive studies of the widths for the PI-AI in He*-Na and He*-K collisions that have been reported[13,14] can serve as an interesting testing ground for the present calculations. Briefly, the shape and magnitude of the width function are quite similar to those for Na and K targets at internuclear separations $R \geq 6a_0$. At smaller

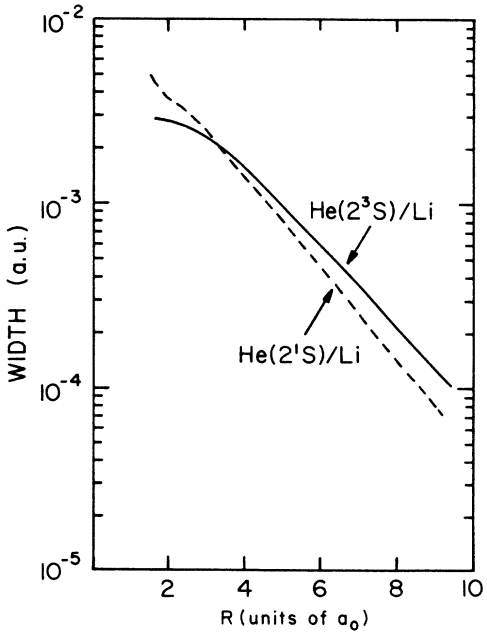

FIG. 3. Autoionization widths for He($2\,^3S$) Li and He($2\,^1S$) Li.

R, where the characteristics of the constituent atoms become more distinctive, differences in structure and magnitude are apparent.

B. IPF and PI-AI mechanisms

For an initial state [He($2\,^3S$)+Li; 1Σ], the collision history of probabilities for the [He+Li$^+$; 0Σ; $\epsilon=0.02$ a.u., $l=m=0$] and [He($2\,^1S$)+Li; 2Σ] channels is displayed in Fig. 4 as a function of time and R, at 0.7 keV and impact parameter $b=3a_0$, in order to illustrate the IPS and PI-AI mechanisms. The 2Σ state is a first step on the ladder leading to IPF.

First, let us examine characteristics of the 2Σ probability in conjunction with the adiabatic potentials in Fig. 1. The 2Σ probability increases abruptly when the particles approach $t\simeq -12$ a.u. (or $R\simeq 7a_0$) on the incoming part of the collision trajectory because of strong radial coupling with 1Σ. A similar increase in the probability occurs at the same R, but on the outgoing part of the collision trajectory, again due to the interaction with 1Σ. At larger $R\geq 7a_0$, the 2Σ probability decreases because of flux promotion that leads to IPF through a series of radial couplings at rather large internuclear separations (a ladder-climbing mechanism). A structure seen in the 2Σ at $t=-10$ a.u. on the incoming part of the collision trajectory is due to the strong coupling with the 1Σ state. Contributions from rotational couplings (via Π states) serves mainly to redistribute the flux within a given n state and hence play a secondary roll in flux promotion.

Next, let us discuss characteristics of the 0Σ probability. Since all states considered here are embedded in the PI-AI continuum, ionization can occur without any change of electronic energy throughout the collision. However, as is clear in Fig. 3, the widths (autoionization rates), and hence, the discrete-continuum coupling matrix elements, are appreciable at small $R\lesssim(6-7)a_0$, so that ionization is effectively limited to trajectories in which the colliding particles approach to within this range. Hence the 0Σ probability increases sharply at nearly the same separations as does the 2Σ probability, and shows very weak structure at $R\leq 5a_0$ that is due mainly to continuum-continuum interactions. However, the structure in the 0Σ state is much weaker than that of the 2Σ state.

On the basis of this apparent competition between the IPF and PI-AI processes at $R\simeq 6a_0$, one might expect interference between the two channels at a specific impact parameter and energy. However, the ejected electron is rather energetic and hence its back-coupling is small, so it is not surprising that the interference is very weak.

TABLE I. The IPF cross section.

E (keV)	IPF cross section (cm^2) initial channel [He($2\,^1S$)+Li]	[He($2\,^3S$)+Li]
0.1	3.5×10^{-20}	1.9×10^{-20}
0.5	9.7×10^{-18}	7.2×10^{-18}
1.0	3.7×10^{-17}	3.2×10^{-17}

C. Cross sections

The calculated cross sections for both the IPF and PI-AI processes are illustrated in Fig. 5 along with the measurement by Neynaber and co-workers.[5] Representative results of the IPF cross section are given in Table I. The PI-AI cross sections result predominantly from the [He($2\,^1S$)+Li] channel. The experiment was actually conducted with a mixture of 87% He($2\,^3S$) and 13% He($2\,^1S$) atoms. Thus our theoretical rate is properly weighted for this comparison. Because our model cannot distinguish the PI and AI channels, Fig. 5 shows the sum

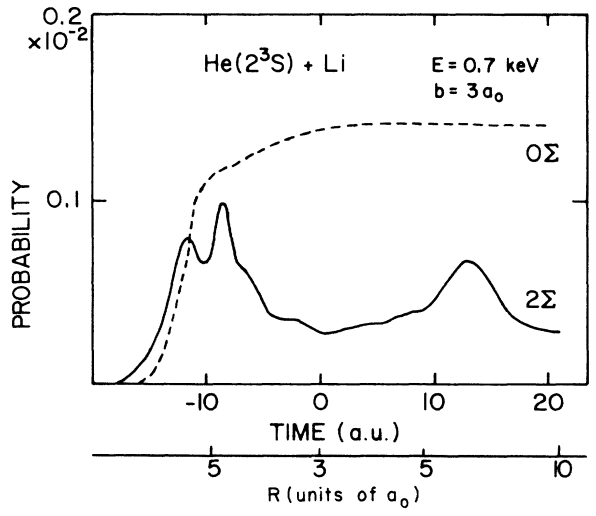

FIG. 4. Time evolution of transition probabilities for [He+Li$^+$; 0Σ; $\epsilon=0.02$ a.u., $l=m=0$] and [He($2\,^1S$)+Li; 2Σ] at 0.7 keV and $b=3.0a_0$.

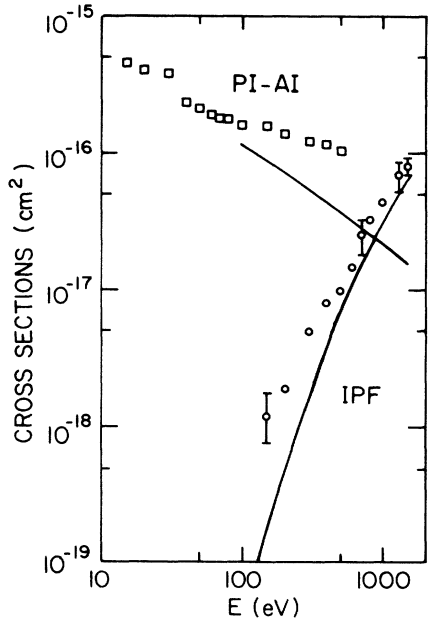

FIG. 5. Cross sections of the IPF and PI-AI as a function of collision energy. Solid lines, present theory. Symbols, experiment, Ref. 5.

of both processes. However, for the collision energies studied here AI is expected to be weak.[5] Experimentally, the PI was found to be dominant and the AI to amount to no more than a few percent of total chemi-ionization.[5] In comparing the present theoretical results and the measurements,[5] the following remarks are in order.

(i) The present IPF cross sections are smaller in magnitude than the measured values at all energies, but they approach the experimental cross section rather rapidly above 0.9 keV. Furthermore, the theoretical cross sections appear to exhibit a change of slope at higher energies ($E \geq 500$ eV), in agreement with the measurement.

(ii) The present PI-AI cross sections are also smaller than the measurement, particularly above 100 eV. The PI-AI cross section is rather sensitive to the discrete-continuum matrix elements, hence the width, and to the $[He+Li^+]$ potential, and a more accurate molecular structure calculation may be necessary in order to obtain more accurate results.

These departures of the theoretical results from the measurement at higher energies are due partly to our model, which assumes that only the $He(2\,^3S)$ and $He(2\,^1S)$ states are exit channels leading to PI-AI. As the energy increases, more flux is promoted to Rydberg levels; consequently, flux may be transferred to ionization channels from these Rydberg levels. This effect is not included in the present calculation, and it could cause an overestimation of the IPF cross section and underestimation of the PI-AI cross section at higher energies. This observation seems to be consistent with the present model. Also, Wang, Tang, and Neynaber[5] noted uncertainty in the composition of the $He(2\,^3S)$ and $He(2\,^1S)$ mixture in their experiment and it is possible that this could contribute to increased discrepancy between the theory and measurement.

IV. SUMMARY AND CONCLUDING REMARKS

The processes of IPF and PI-AI in $He^*(2\,^{1,3}S)+Li$ collisions have been studied theoretically by using a molecular-orbital expansion method (including MO-ETF) within a semiclassical scattering formalism. Because of the weak polarization interaction between the colliding particles and, as a result, the absence of avoided curve crossings and strong radial couplings, the IPF process has a small cross section of the order of 10^{-20} cm^2 at 0.1 keV. However, the cross section increases rather sharply as the energy increases and attains a value of 3.3×10^{-17} cm^2 at 1 keV. On the other hand, PI-AI is always energetically possible with no change in electronic energy; hence it has a large cross section of the order of 10^{-16} cm^2 at 0.1 keV, which decreases as the energy increases to 2×10^{-17} cm^2 at 1 keV. Although the very weak interference between the IPF and PI-AI was theoretically found in the region where these processes become equally probable, experimentally it may be rather difficult to detect.

Recently, Merz *et al.*[15] measured the ejected-electron energy spectra arising from the PI in $He^*(2\,^{1,3}S)+Li$ collisions in the $E \leq 1$-eV region, demonstrating the importance of electron angular-distribution effects on the spectra of attractive PI systems. Their findings pose interesting questions about the collision dynamics of the PI process, in particular, the transfer of angular momentum between the rotating quasimolecule and the ejected electron, which await complete theoretical interpretation. We plan to study these measured results of the ejected-electron energy spectra and angular distribution by employing a quantum-mechanical approach.

ACKNOWLEDGMENTS

This work was supported in part by the U.S. Department of Energy, Assistant Secretary for Energy Research, Office of Health and Environmental Research, under Contract No. W-31-109-Eng-38 (M.K.), the Office of Basic Energy Sciences, Division of Chemical Sciences (N.F.L.), and the Robert A. Welch Foundation (N.F.L.).

[1]R. E. Olson, M. Kimura, and H. Sato, Phys. Rev. A **30**, 1692 (1984).
[2]R. E. Olson and M. Kimura, Phys. Rev. A **32**, 3092 (1985).
[3]K. Miethe, T. Dreisiedler, and E. Salzborn, J. Phys. B **15**, 3069 (1982).
[4]A. M. Howald, R. E. Miers, J. S. Allen, L. W. Anderson, and C. C. Lin, Phys. Rev. A **29**, 1083 (1984).
[5]D. P. Wang, S. Y. Tang, and R. H. Neynaber, J. Phys. B **20**, 1527 (1987).
[6]S. Y. Tang, D. P. Wang, and R. H. Neynaber, J. Phys. B **20**, L85 (1987).
[7]M. Kimura and N. F. Lane, in *Advances in Atomic, Molecular, and Optical Physics* (Academic, New York, 1989), Vol. 26, p. 79.
[8]J. N. Bardsley, Case Stud. At. Phys. **4**, 299 (1974).
[9]M. Krauss, P. Maldonado, and A. C. Wahl, J. Chem. Phys. **54**, 4944 (1971).
[10]W. J. Stevens, A. M. Karo, and J. R. Hiskes, J. Chem. Phys. **74**, 3989 (1981).
[11]M. Kimura and N. F. Lane, Phys. Rev. Lett. **52**, 2160 (1986).
[12]T. F. O'Malley, Phys. Rev. **150**, 14 (1966).
[13]J. S. Cohen, R. L. Martin, and N. F. Lane, Phys. Rev. A **31**, 152 (1985).
[14]K. F. Scheibner, J. S. Cohen, R. L. Martin, and N. F. Lane, Phys. Rev. A **36**, 2633 (1987).
[15]A. Merz, M. W. Müller, M. W. Ruf, H. Hotop, W. Meyer, and M. Move, Chem. Phys. Lett. **160**, 377 (1989).